IEEE Access
Multidisciplinary ⋮ Rapid Review ⋮ Open Access Journal

Received 20 December 2024, accepted 6 January 2025, date of publication 13 January 2025, date of current version 23 January 2025.

Digital Object Identifier 10.1109/ACCESS.2025.3528871

RESEARCH ARTICLE

Power Transmission for Millimeter-Wave Indoor/Outdoor Wearable IoT Devices Using Grounded Coplanar Waveguide-Fed On-Body Antenna

FUAD ERMAN[1,2], SLAWOMIR KOZIEL[2,3], (Fellow, IEEE), ALHARETH ZYOUD[4], (Member, IEEE), LEIFUR LEIFSSON[5], UBAID ULLAH[6], (Senior Member, IEEE), AND SHAKER ALKARAKI[7], (Member, IEEE)

[1]College of Telecommunications and Information Technology, Nablus University for Vocational and Technical Education, Nablus 110, Palestine
[2]Engineering Optimization and Modeling Center, Reykjavik University, 102 Reykjavik, Iceland
[3]Faculty of Electronics, Telecommunications and Informatics, Gdansk University of Technology, 80-233 Gdańsk, Poland
[4]Department of Electrical and Computer Engineering, Birzeit University, Ramallah 14, Palestine
[5]School of Aeronautics and Astronautics, Purdue University, West Lafayette, IN 47907, USA
[6]Networks and Communication Engineering Department, Al Ain University, Abu Dhabi, United Arab Emirates
[7]Department of Electrical Engineering, George Green Institute for Electromagnetic Research, University of Nottingham, NG7 2RD Nottingham, U.K.

Corresponding author: Fuad Erman (erman@nu-vte.edu.ps)

This work was supported in part by the Nablus University for Vocational and Technical Education, in part by the Icelandic Research Fund under Grant 239858, and in part by the National Science Centre of Poland under Grant 2020/37/B/ST7/01448.

ABSTRACT This paper presents for the first-time evaluation of wireless power transmission (WPT) for sustainable low-powered Internet of Things (IoT) devices in realistic indoor/outdoor scenarios using empirical propagation models at 28 GHz. The used empirical propagation models have shown that using an on-body 9×9 mm-wave rectenna array based on a proposed mm-wave antenna is able to charge IoT devices at a distance of 57 m for line-of-sight (LOS) indoor temporal environment, and at a distance of 10 m for LOS outdoor tropical propagation model using a base station with 53 dBm transmission power. Furthermore, the mm-wave on-body 9×9 rectenna array occupies an area equal to that of a single UHF rectenna, while collecting 17-fold more power. In addition, the article discusses the design and experimental results of a single-element on-body mm-wave antenna used to design the 9×9 rectenna array. The proposed mm-wave antenna is a single-layer low-profile structure. Furthermore, the antenna has a stable gain of over 9.5 dBi and a wide beamwidth. The on-body antenna structure consists of rectangular multi-slot patch fed by a 50 Ω grounded coplanar waveguide (GCPW) line. Employing the multi-slot configuration results in a wearable antenna's impedance bandwidth of 3.73 GHz. The peak measured gain of the antenna is 10.5 for chest/arm-mounted case in the operating 28 GHz N257 5G band. The antenna's radiation pattern forms a wide off-body forward direction beam. A prototype of the proposed antenna is fabricated and validated experimentally for both cases on a human volunteer arm/chest and in the free space. The size of the proposed structure is small and can collect power with high efficiency due to the short wavelength of millimeter wave (mm-wave) in contrast to UHF antennas.

INDEX TERMS Antennas, energy harvesting (EH), millimeter-wave (mm-wave), rectenna, wireless power transfer (WPT).

I. INTRODUCTION

Utilization of millimeter wave (mm-wave) bands has led to a revolutionary development in sensing applications, wireless

The associate editor coordinating the review of this manuscript and approving it for publication was Feng Wei.

body area networks (WBAN), and Internet-of-Things (IoT) [1], [2], [3]. Antennas operating at 28 GHz band have enabled high-speed of data transmission and high-quality wireless communication, wireless power transfer (WPT), as well as massive mm-wave IoT connectivity [4], [5], along with the detection of moving objects [6]. The migration toward the mm-wave band facilitates obtaining higher gain for a given physical space occupied by the antenna [7]. This has fostered investigation of the theoretical [8], [9] and practical [10], [11] aspects of mm-wave WPT for IoT applications.

IoT WBAN applications have been pursued in the mm-wave band, including defence, fitness tracking, healthcare monitoring, and wearable sensing [6], [12]. Significant interest has been observed in researching possibilities of powering such systems using microwave and mm-wave rectennas, from ultra-high frequency (UHF) to mm-wave 5G bands [4], [13], [14]. WPT is a scalable and reliable method increasingly employed for powering IoT devices [15]. Moreover, the compactness and portability of body-worn devices are required for IoT WBAN. From this point of view, a single-layer antennas with small physical size, wide impedance bandwidth, stable beam, wide beamwidth, and low back radiation are indispensable [16]. In the literature, different mm-wave antenna featuring various topological configurations have been reported. However, bulky structures hinder their wearable applicability for long-term purposes [17], [18], [19], [20], [21], [22], [23]. Antenna compactness is a crucial consideration for practical applications.

An improved-efficiency WPT can be accomplished at mm-wave bands due to higher antenna gain [2]. A compact/large area rectenna analytically shows sufficient power for charging wearable, portable, and low-powered IoT devices at high frequencies above 20 GHz [24]. Therein, in practical scenarios, the following three important factors should be considered: the targeted voltage level (i.e., sufficient power density), fabrication cost, and rectenna size. A trade-off always arises between the performance and the rectenna size [25], [26]. In many countries, new regulations for RF WPT are still being developed. This paper contributes to these efforts. The evaluation of charging low-powered IoT devices based on single/array rectennas has not been investigated in realistic indoor/outdoor scenarios using an empirical propagation model at 28 GHz. In addition, the analytical comparison is not introduced to a similarly sized UHF counterpart. Consequently, our upfront goal is to design a wearable on-body antenna suitable for mm-wave WPT and extensively investigate its performance in realistic indoor/outdoor scenarios.

In this research article, a low-profile mm-wave antenna featuring simple topological structure, compact size, stable radiation pattern, high gain, and wide impedance bandwidth has been developed. A 50 Ω grounded coplanar waveguide (GCPW) feeding line is utilised to feed a rectangular multi-slot patch antenna. The radiation elements are allocated on the upper side of the substrate, whereas the backside is fully covered with copper to limit the backside radiation. The suggested structure is constructed on a single layer of Rogers RO4003C substrate. Embedding three different narrow slots of diverse dimensions along with the x-axis ensures wide operating bandwidth of the proposed antenna. In particular, the impedance bandwidth centered at 28 GHz is 3.73 GHz, which covers the N257 band. The antenna has a measured stable in-band gain exceeds 9.5 dBi over the entire bandwidth. The simulation results are validated experimentally, where the suggested antenna is evaluated in the free space and while mounted on the body (chest/arm) of the volunteer. The peak measured gain is 11 dBi in the free space and 10.5 dBi for the chest/arm-mounted case in the operation band of N257. Then low profile-topology antenna is employed for sustainable low-powered mm-wave IoT devices. The evaluation of WPT is conducted for realistic indoor/outdoor scenarios using empirical propagation models at a frequency of 28 GHz. In more detail, the proposed antenna is arranged into a 9×9 rectenna array, which collects power almost 17 times higher than the UHF antenna of the same size. In addition, our evaluation shows that a base station with 53 dBm transmission power charges the rectenna array at 57 m coverage distance for the line-of-sight (LOS) indoor temporal propagation model and at 10 m for the LOS outdoor tropical propagation model. This result promises sustainable mm-wave-powered IoT devices, especially in the indoor temporal region. The structure of this research paper is arranged in the following way: Section II discusses the design and simulation of the proposed single-port antenna. Section III introduces the design stages and analysis of the proposed antenna to describe how to achieve the targeted characteristics. Then, the simulation and measurement results of the proposed antenna are presented in the experimental validation section. Finally, the proposed antenna is used to evaluate the WPT for sustainable low-powered IoT devices in realistic scenarios using empirical propagation models at 28 GHz is demonstrated.

II. DESIGN AND SIMULATION OF A SINGLE-PORT ANTENNA

A. ANTENNA STRUCTURE

Figure 1 shows the geometry and schematics of the proposed mm-wave wearable antenna. The antenna is designed for energy harvesting (EH) at mm-wave bands, where maintaining a broad impedance bandwidth is a necessity. The mm-wave penetration capabilities of tissue beyond the skin are poor [27], and appropriate radiation pattern is a prerequisite to support off-body communication. The designed antenna should feature a wide beamwidth to harvest energy efficiently due to the wide variation in the incident angle of power. The proposed wearable antenna (length: $S_y = 30mm$, width: $S_x = 10mm$) consists of a single-layer low-profile structure fabricated on Rogers RO4003C substrate. The RO4003C slab has a dielectric constant of 3.38 and thickness of 0.508 mm. In addition, a 50 Ω GCPW feeding line is used to excite a rectangular multi-slot patch antenna

($L_p = 17.5\ mm$ and $W_p = 9mm$) as shown in Fig. 1(a). In fact, the multi-slot patch can be considered as a low-profile antenna where the coplanar ground planes exist on both side of the feeding line. Three different narrow slots along with the x-axis are embedded into the rectangular patch with different dimensions ($W_1 = 1.1$, $L_1 = 6$, $W_2 = 1.5$, $L_2 = 7$, $W_3 = 1.5$, and $L_3 = 8$). Etching these slots improve significantly the impedance bandwidth of the proposed antenna. In fact, employing the multi-slot configuration effectively excites multimode resonances with close frequencies that effectively enhance the bandwidth of the antenna. The radiation elements are allocated on the upper side of the substrate, whereas the backside consists of a full ground plane order to limit the backside radiation. The antenna is fabricated and is fed using 2.92mm Southwest end-launch connector as shown in Fig. 1(b), making the proposed antenna suitable for portable applications.

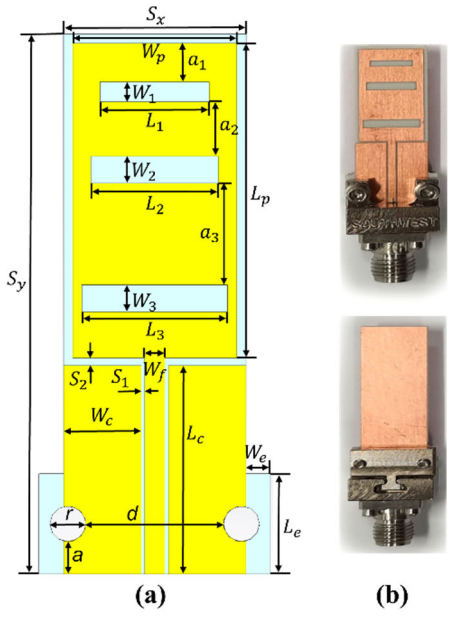

FIGURE 1. Geometry of the designed low-profile mm-wave antenna $W_f = 1.1$, $W_p = 9$, $L_p = 17.5$, $W_1 = 1.1$, $L_1 = 6$, $W_2 = 1.5$, $L_2 = 7$, $W_3 = 1.5$, $L_3 = 8$, $a = 1.8$, $a_1 = 2.15$, $a_2 = 3.025$, $a_3 = 5.65$, $S_1 = 0.2$, $S_2 = 0.4$, $W_c = 4.25$, $L_c = 11.6$, $W_e = 1.35$, $L_e = 5.58$, $d = 7.55$, $r = 1.98$, $S_x = 10$, $S_y = 30$ (a) Parameterized front view (b) Front and back view of fabricated prototype. (Yellow: copper, Cyan/Gray: substrate).

B. DESIGN STAGES AND ANALYSIS

The proposed mm-wave antenna is analyzed and simulated using CST Microwave Studio. The mm-wave wearable antenna is designed to operate on 28 GHz N257 band. Parametric analysis of the design variables, for instance, the size of the patch and embedded slots as well as the distance between the embedded slots, is crucial to realize the desired characteristics. Initially, the simulation starts with a structure that includes a feed line flanked by coplanar ground planes at both sides and a rectangular patch referred to as Ant-1 as showcased in Fig. 2(a). At this stage, Ant-1 is a conventional patch antenna with a single resonant frequency at 28.5 GHz and a −10-dB bandwidth of 206 MHz as shown in Fig. 2 (b). The TM_{23} patch is designed with $L_p = 17.5\ mm$ and $W_p = 9mm$. For planar microstrip cavity (i.e., $t \ll \lambda$), the transverse magnetic (TM) mode can be computed using the dimensions of the rectangular patch, specifically its width and length [28]. The resonant frequency (f_{mn}) of a TM_{mn} mode is expressed as

$$f_{mn} = (K_{mn}c)/(2\pi\sqrt{\epsilon_r}) \quad (1)$$

$$k_{mn} = \sqrt{(m\pi/L_p)^2 + (n\pi/W_p)^2} \quad (2)$$

where the speed of light is denoted as c. f_{mn} and k_{mn} refer to the resonant frequency and wavenumber for the mn mode respectively, whereas it has computed using the patch dimensions [28]. L_p and W_p are the length and width of the patch on the m and n respective axes.

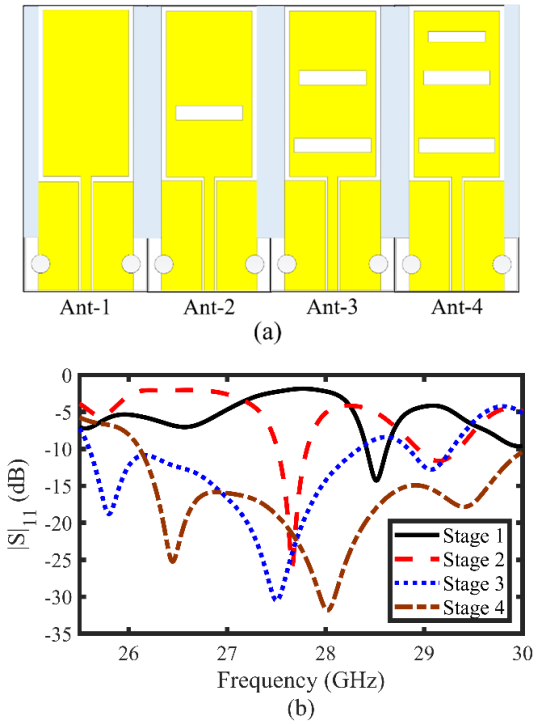

FIGURE 2. Proposed antenna: (a) design stages of the GCPW-fed wearable structure, (b) S_{11} response for each design stage.

The impedance bandwidth of Ant-1 is improved with the addition of each horizontal slot due to the excitation of extra resonances. The first slot is added to the center of the patch as shown in Fig. 2(a) shows a new resonant frequency at 27.66 GHz. In more detail, the position and dimensions ($W_2 = 1.5$ and $L_2 = 7$) of the embedded slot, located in the middle of the radiating patch, are precisely chosen to expand the impedance bandwidth. The antenna with one central slot, referred to as Ant-2, has a −10-dB impedance bandwidth of approximately 715 MHz as shown in Fig. 2(b). Similarly, a second slot is added and an extra resonance is excited at 25.8 GHz, and the respective antenna is referred to as Ant-3.

Optimizing the position and dimensions of the second slot led the antenna improving its bandwidth by additional 2.6 MHz, which is now 3.3 GHz, as shown in Fig. 2(b). Finally, the addition of the third horizontal slot on top of the radiating patch improves the −10-dB impedance bandwidth of the antenna and the lower S_{11} response, covering the desired operating 28 GHz N257 band. The resulting antenna is named Ant-4 as shown in Fig. 2(a). Ant-4 has a −10-dB impedance bandwidth of 3.73 GHz ranging from 26.32 GHz to 29.82 GHz as shown in Fig. 2(b). The three different narrow slots are arranged as one radiator due to the smaller distance between the slot radiators than that conventional slot-array elements. In addition, the proposed antenna is not gradually expanding periodic structure; it is a multi-slot configuration introducing multimode resonances eventually leading to a broadband characteristic. To conclude the design procedure, the proper adjustment of slots' position, length, and width is carried out, which enables achieving the reflection response covering the target bandwidth from 26.5 GHz to 29.5 GHz. Furthermore, to ensure that the antenna is applicable to WPT, the voltage standing wave ratio (VSWR) should be kept less than 2 not to jeopardize other system components.

III. EXPERIMENTAL VALIDATION

This section presents the measured and simulated results of the proposed antenna. The antenna has been tested in the free space as well as on the arm and chest of a human volunteer in the Reykjavik University anechoic chamber as shown in Fig. 3. The measured and simulated results are analyzed using the antenna measurement procedures compliant with the IEEE standard [IEEE Std149-1979 (R2008)]. Different scenarios are followed to evaluate the proposed structure performance in terms of S_{11} response, specific absorption rate (SAR), realized gain (G_r), radiation efficiency as well as E- and H-plane patterns. This includes simulation and measurement in the free space and on-body both on the arm and chest. The fabricated prototype is worn with a few millimeters of separation from the human skin for on-body (arm / chest) measurement results (the prototype is hung up $\sim$ 3.5 mm away from the human body as seen in Fig. 3 (b) and (c)).

The antenna's specific absorption rate (SAR) is tested as shown in Fig. 3(d) and (e), while the designed antenna is mounted on-body either the arm or chest of the human model. The values of SAR are around 1.07 and 0.00267 W/kg on chest and arm, respectively. The obtained SAR values are compliant with the safety standard of IEEE (below of 1.6 W/kg). In addition, the antenna's S_{11} is required to maintain its bandwidth in the proximity of the human subject. Also, the impedance matching response should be unaffected by the presence of human body. The proposed antenna has a measured −10-dB bandwidth of 3.65 GHz ranging from 26.1 GHz and 29.75 GHz as shown in Fig. 4. It is observed that S_{11} response in on-body scenarios and free space case are very close to each other and the reflection levels are lower than −10-dB for all evaluation cases over the same operating bandwidth, from 26.5 GHz to 29.5 GHz. Furthermore,

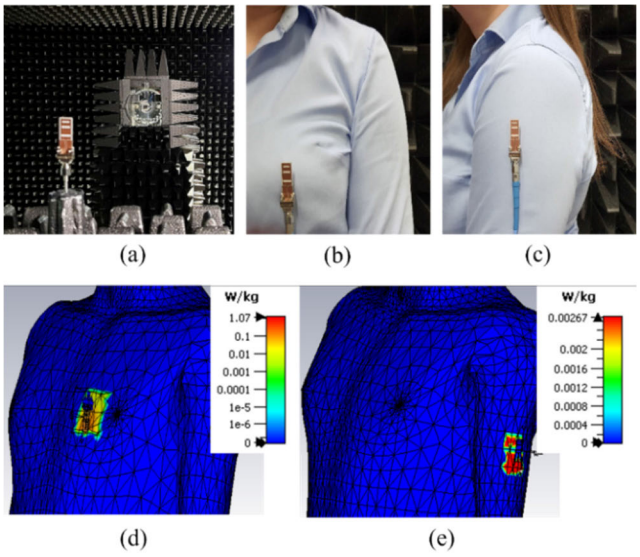

FIGURE 3. Experimental validation of the proposed antenna: (a) measurement setup of the proposed antenna in an anechoic chamber, (b) antenna on chest. (c) antenna on arm, (d) simulation model for SAR on chest, (e) simulation model for SAR on arm.

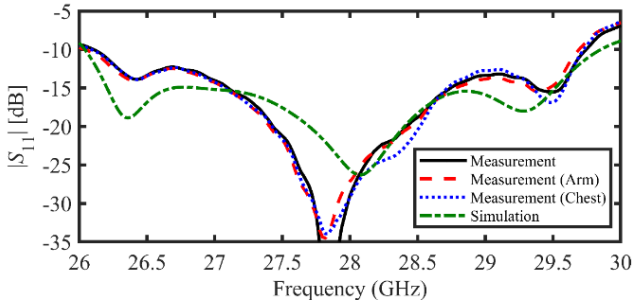

FIGURE 4. The simulation and measurement of S_{11} response of the proposed single-layer antenna.

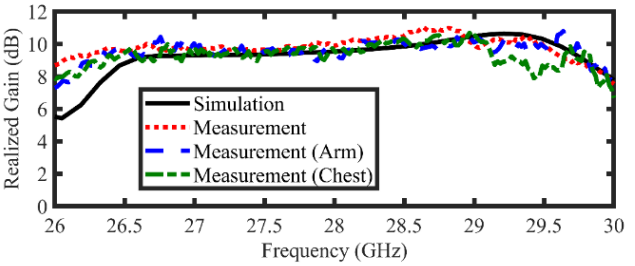

FIGURE 5. The simulation and measurement of antenna's realized gain.

a minor shift of 238 MHz in the resonance frequency is observed between the measured and simulated S_{11} of the proposed antenna due to fabrication tolerances.

The antenna gain is analyzed in the free space and chest/arm-mounted case. It is worth mentioning that the gain performance is stable over entire operating bandwidth as indicated in Fig. 5. The peak measured gain is 11 dBi at 28.6 GHz and the gain curve is higher than 10 dBi for the entire operation bandwidth in the free space as shown in

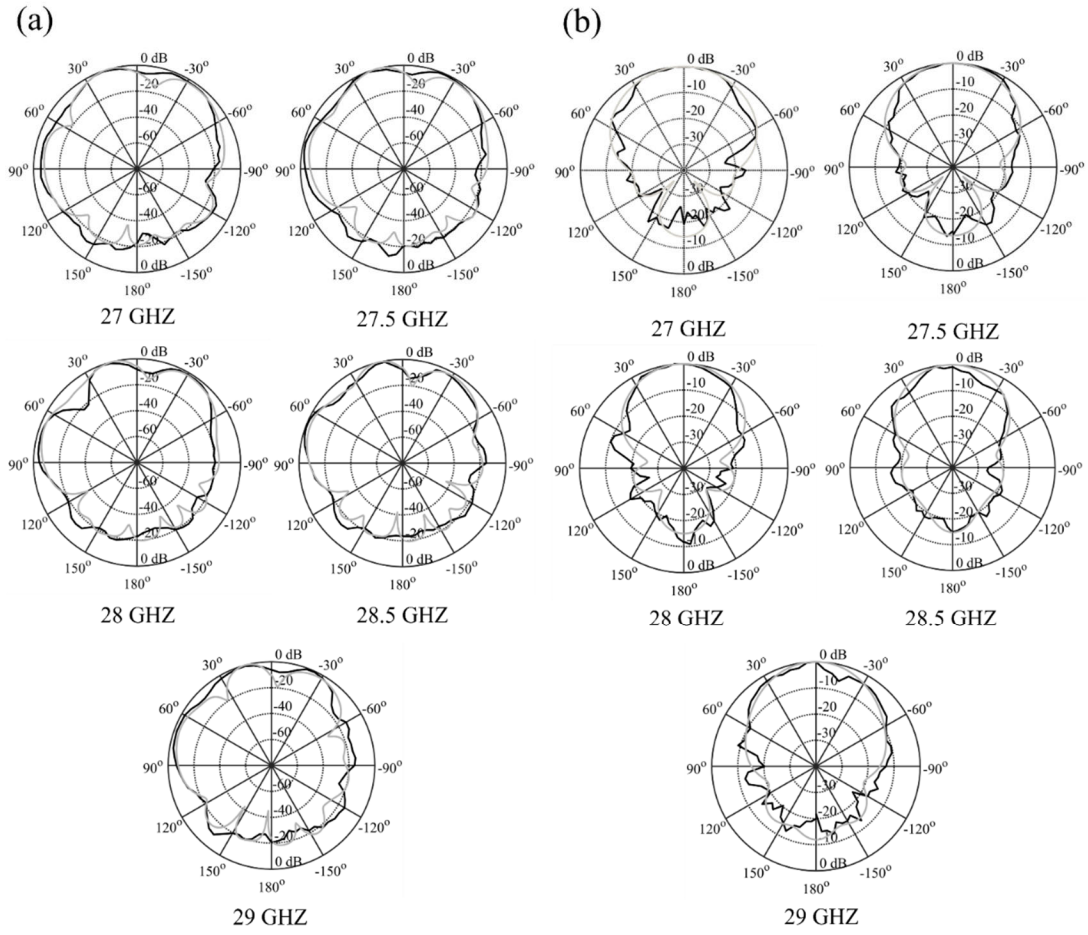

FIGURE 6. Measured (black) and simulated (gray) far-field radiation patterns (a) E-plane and (b) H-plane at 27, 27.5, 28, 28.5, and 29 GHz.

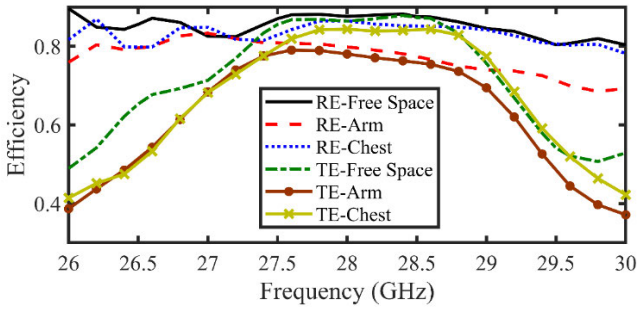

FIGURE 7. The computed RE and TE of the designed wearable antenna on arm, chest, and in free space.

Fig. 5. The peak value of gain is 10.5 dBi at 28.9 GHz for chest/arm-mounted case as depicted in Fig. 5. The gain curves for chest/arm-mounted case are nearly stable around 10 dBi with a marginal ±0.5 dB in-band fluctuation. In fact, the back side of the substrate is a full laminate with copper, which increases the structure's immunity to human body, guaranteeing low-back radiation, with most of the energy radiated away from the body. However, losing a part of antenna's power due to the presence of human tissues is still an issue, eventually leading to a slight degradation of the gain. Furthermore, the antenna performance is evaluated using radiation efficiency (RE) and total efficiency (TE) for body-centric application. Figure 6 exhibits the antenna's RE and TE on the body and free space. The peak RE is 86.5% at 28 GHz when the designed antenna is worn on the chest, while the RE is 83.3% at 27 GHz on the arm and it is 88.1% at 27.8 GHz in the free space. The lowest RE value is approximately 71% at 29.5 GHz, cutoff frequency, when the antenna is worn on the volunteer's arm as seen in Fig. 6 at the edge of impedance bandwidth. In addition, it was observed that the computed TE of the antenna is 84.3% and 87.8% when the antenna is worn on the chest and in free space respectively as seen in Fig. 6.

The measured and simulated far-field radiation patterns in E-plane and H-plane are shown in Fig. 7. The proposed structure possesses a wide angular coverage (i.e., −10-dB beamwidth), which facilitates energy harvesting and may only lead to small deviations in acquired power around the broadside direction as seen in Fig. 7. This is unlike the pencil-like beams observed in conventional arrays structure. In both planes, stable power transmission can be observed

for the entire operating band, achieved within a stable wide beam. This demonstrates that although the antenna naturally features omnidirectional radiation pattern, it can be reshaped into a wide directional beam. The front-to-back ratio is better than 13 dB at 28 GHz. The shape of the antenna's main lobe is enabling more position-tolerant EH on the z-axis [29].

A comparison between the performance of the proposed antenna and other state-of-art antennas has been shown in Table 1. It is worth mentioning that to date, few works have been reported on the 28 GHz range for wearable applications. A comparison in terms of the number of layers, impedance bandwidth, peak gain, and size, indicate that the proposed structure performance is offers a competitive edge over the reported works. In particular, the impedance bandwidth and realized gain are comparable and, in some instances better than for the benchmark designs. In addition, a simple construction of our structure facilitates the fabrication process and meets the requirement of low-profile structures applications.

TABLE 1. Comparison between the performance of the proposed antenna and state-of-art antennas reported in the literature.

Ref	Dimension (mm)	Freq (GHz)	BW (GHz)	Gain (dBi)	No. of Layers	Tested On-Body
[16]	29.08 × 11.42 × 0.508	28	2	11.7	1	Yes
[17]	27 × 27 × 0.254	24	0.8	6	2	Yes
[18]	75 × 12.5 × 1.5	24	1	-	1	No
[19]	28.7 × 13 × 2.5	28	3.05	11.65	4	Yes
[20]	63 × 63 × 0.79	10	0.55	12	1	No
[21]	33.6 × 28.6 × 0.7	24, 28	10.53	8.4, 7.9	2	Yes
		38	6.2	10.3		
[22]	67 × 44 × 0.254	28	2.3	12.6	1	Yes
[23]	80 × 80	3.5, 5.8	0.62, 0.6	8.37, 6.55	2	Yes
[24]	36 × 11.4 × 0.42	26	6.2	8.9	1	Yes
[30]	12 × 3 × 0.25	28, 38	0.68, 0.86	6.11, 7.15	1	Yes
This Work	30 × 10 × 0.508	28	3.73	11	1	Yes

IV. POWER TRANSMISSION FOR MILLIMETER-WAVE INDOOR/OUTDOOR WEARABLE IOT DEVICES

In this section, the evaluation of the power harvesting performance for different propagation models based on the proposed on-body antenna is presented. The following three important parameters, the targeted voltage level, fabrication cost, and rectenna size, should be taken into account when implementing IoT devices. The received voltage level and rectenna size will be investigated here.

The receiver of a limited size can acquire higher power in mm-wave bands. This has motivated the design of miniaturized RF-power devices for mm-wave bands (above 20 GHz) due to the improvement in the antenna size to wavelength ratio for area-constrained devices [10]. The forward transmission coefficient (S_{21}) is measured between two copies of the proposed antennas connected to the VNA's ports, as shown in Fig. 8(a). Both antennas are positioned at distance of 50 cm from each other to perform the measurement in the far field as seen in Fig. 8(b). Figure 8(c) shows the measured S_{21} from 26 GHz to 30 GHz. The measured S_{21} demonstrates that in mm-wave band the antenna's performance (gain / efficiency) is improved in contrast with UHF ISM band (2.4 GHz) despite the increased path loss. The proposed antenna is able to realize over 10−20 dB higher S_{21} within the operating bandwidth of the 28 GHz N257 band [24].

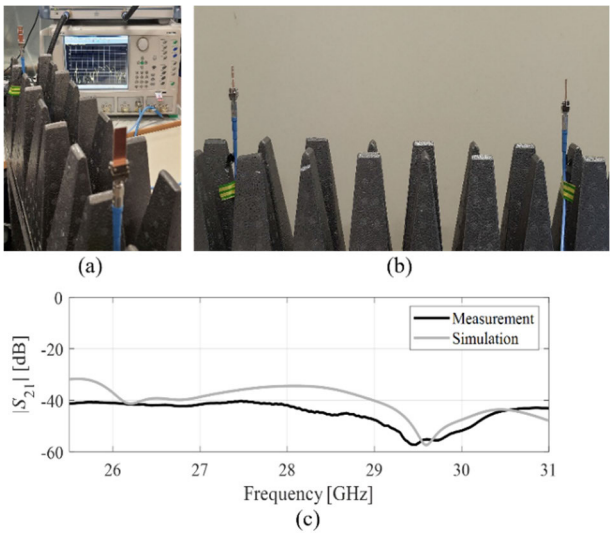

FIGURE 8. Path gain measurement: (a) setup, (b) picture indicating the distance of 50 cm between two symmetric antennas (designed antenna), and (c) the measured path gain (S_{21}).

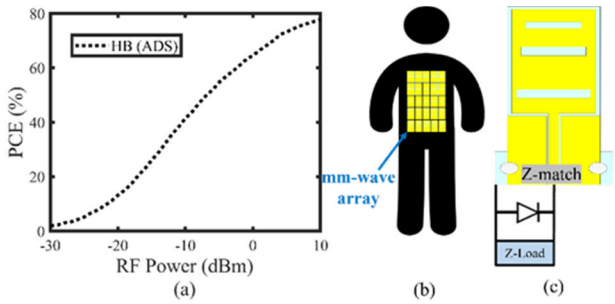

FIGURE 9. (a) The PCE of HB simulation at 28 GHz. (b) The architecture of large-area rectenna array. (c) The rectenna's structure.

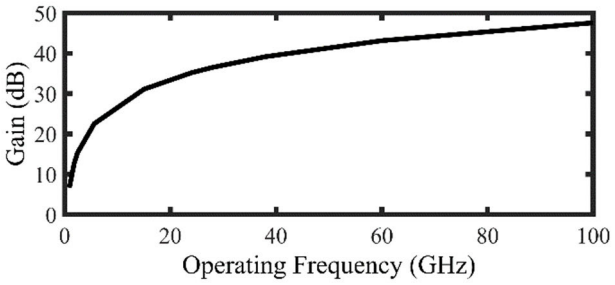

FIGURE 10. Antenna's gain as a function of the operating frequency for fixed physical aperture area and efficiency.

The low-profile substrate and ability to implement off-body communication are additional advantages of employing patch antennas for WPT in mm-wave bands.

The most common method for evaluating power conversion efficiency (PCE) in mm-wave EH network is harmonic balance (HB) simulation, which provides a conservative estimate compared to other models such as linear, nonlinear and quadratic [31]. This method is particularly well-suited for accurately reflecting losses due to the generation of harmonics at very low power levels, as observed in the analytical diode PCE formulas [32]. In this work, the VDI W-band ZBD GaAs Schottky diode is employed. This diode features a parasitic capacitance and low forward voltage, making it suitable for low-power rectification (up to 100 GHz) [33]. The calculated PCE is presented in Fig. 9(a), utilizing HB simulation. In the HB model, a peak PCE of 77% is based on the commercial diode [2].

The 53-dBm value represents the equivalent isotopically radiated power (EIRP) for the transmitter. Maximum permissible EIRP levels in mm-wave bands are higher than sub-5 GHz bands. For instance, the base station in 5G networks can radiate up to 75 dBm, with high-gain phased array antenna with beam scanning abilities being employed to achieve these higher EIRP levels [34]. Below 5 GHz, the limit for EIRP is typically 4 W (approximately 36 dBm). The aperture efficiency e_a is used to theoretically calculate the minimum physical aperture area of antenna A_{Phys} using the following equation,

$$A_{Phys.} = G\lambda^2 \Big/ 4\pi e_a \tag{3}$$

where G is the antenna gain and $\boldsymbol{\lambda}$ is the wavelength. According to (3), the relation of antenna's gain to the operating frequency for a fixed antenna size is shown in Fig. 10. This is due to the improvement in the antenna gain-to-wavelength ratio. Consequently, when an antenna operates at 28 GHz, its size is 96.8% less than an antenna working at 900 MHz based on the exhibited antenna gain in Fig. 10 and aperture efficiency of 90%. Consequently, employing antennas at mm-wave bands results in an increased number of antennas occupying the same area and tolerating more pervasive deployment of IoT devices. Fig. 9(b) shows the architecture of large-area rectenna array, whereas Fig. 9(c) shows the rectenna's structure.

A rectenna array based on the proposed antenna has been analysed, as shown in Fig. 11. Each rectenna is formed using a single element rectifier. The large area rectenna does not result in a more directional radiation pattern, and hence, does not reduce the antennas' harvesting beamwidth. As stated in [35], the losses of DC combination have demonstrated to be at the level of only 1%. The proposed antenna is considered to construct multiple arrays with 5.4 mm (λ/2 at 28 GHz) spacing between the elements. In this section, to maintain a precise representation of the antenna's performance as a wearable receiver of wireless power, the analysis is performed according to the lower measured on-body gain,

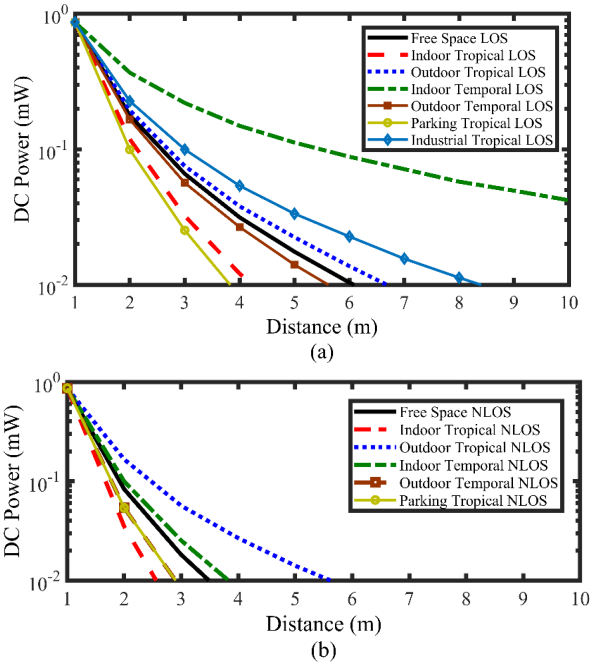

FIGURE 11. The single rectenna element evaluation of received power as a function of distance for different propagation models (a) LOS and (b) NLOS.

9.5 dBi, of the proposed patch antenna within the operating bandwidth. The occupied area of a UHF antenna is 190mm × 240 mm as seen in [36]. This area can be occupied with an 9 × 9 array of the proposed mm-wave rectenna that works at 28 GHz N257 band. This array receives a power almost 17 times higher than that of a UHF rectenna, as shown in Fig. 11. Furthermore, Fig. 11 compares the received power between a compact single rectenna and a different array sizes of mm-wave rectennas in the free space environment. Fig. 11 shows that an 5 × 5 array or larger of the proposed rectenna outperforms the UHF rectenna. This demonstrates that body-centric WPT and off-body source's EH realize better end-to-end efficiency because of the short wavelength of millimeter wave (mm-wave).

The rectenna's received power in dBm and mW, P_{Rx} (dBm) and $P_{Rx}(mW)$, respectively, can be computed as

$$P_{Rx}\,(dBm) = P_{EIRP} + G_{Rx} - 20log_{10}\left(\frac{4\pi f}{c}\right) - 10nlog_{10}\,(d) \tag{4}$$

$$P_{Rx}\,(mW) = 10^{(P_{Rx}(dBm)/10)} \tag{5}$$

where P_{EIRP} is the permissible level of EIRP, G_{Rx} is the gain of receiver antenna, c is the speed of light, f is the operating frequency in Hz, and d is the distance between antenna and base station in meter.

The obtained DC power based on the PCE can be found as

$$P_{Rx}\,(mW)\,DC = P_{Rx}\,(mW) * PCE \tag{6}$$

The harvested power by the rectennas is computed using different propagation models where the consistent value of

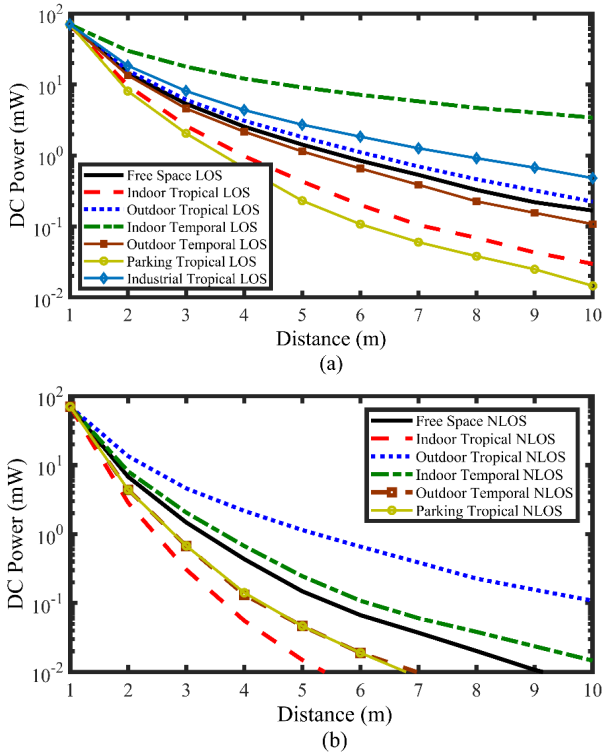

FIGURE 12. An 9 × 9 array rectenna based on the proposed antenna evaluation of received power as a function of distance for different propagation models (a) LOS and (b) NLOS.

TABLE 2. The path loss exponent for different scenarios at 28 GHz.

Scenario	LOS	NLOS	Scenario	LOS	NLOS
Indoor temporal	1.1	2.7	Free space	2	2.8
Outdoor temporal	2.1	3.4	Parking tropical	2.7	3.4
Indoor tropical	2.5	3.85	Industrial tropical	1.7	-
Outdoor tropical	1.9	2.1			

PCE (from HB simulation) with received power is used. To provide a more realistic analysis, various empirical model scenarios, either LOS or non-line-of-sight (NLOS), are used where the path loss exponent value is determined based on real measurements conducted in the literatures [37], [38], [39], [40], [41], and [42], as shown in Table 2.

The performance of rectenna, either as a single element or as an array, is analyzed for low-powered IoT devices and tested in different practical scenarios, including LOS or NLOS, as shown in Figs. 12 and 13, respectively. IoT devices require a minimum power of 0.2 mW to operate in an WBAN case [25]. The evaluation of targeted power (receiving 0.2 mW) as a function of distance is shown in Fig. 12(a) and Fig. 12(b) for single rectenna. Figures 12(a) and 12(b) exhibit the LOS and NLOS scenarios, respectively, for different practical environments. It can be observed that powering wearable IoT devices can be achieved at a maximum distance of 1.7 − 3.2 m for LOS environments and 1.4 − 1.9 m for NLOS environments. An 9 × 9 array of rectenna is analyzed to determine the maximum coverage distance to power an IoT device, as presented in Figs. 13(a) and 13(b) for LOS and NLOS, respectively. The array's size is the same as that of a UHF rectenna. It was found that the maximum distance of a 9 × 9 rectenna array to charge an IoT device in different LOS propagation environments is 57 m for indoor temporal regions, while it is 5.2 m for parking tropical environments. For NLOS environments, it is possible to charge the IoT device at 8 m for outdoor tropical regions, whereas the distance is 3 m for indoor tropical regions. This indicates that utilizing large area wearable IoT devices improves the charging distance two-fold for indoor NLOS environments and four-fold for the outdoor NLOS environment. Additionally, the IoT device charging distance is increased 3-fold for the LOS parking tropical scenario and 18-fold for the LOS indoor temporal scenario. Despite higher path loss at mm-wave bands, the WPT efficiency is improved and powering IoT device area is expanded. According to this analysis, WPT can be used beneficially in indoor temporal region due to the coverage distance.

V. CONCLUSION

This article presents an evaluation of powering low-power IoT devices in realistic indoor and outdoor scenarios using empirical propagation models at 28 GHz. The evaluation is assessed based on the designed on-body mm-wave antenna, used to construct a 9 × 9 mm-wave rectenna array occupying the same area as a single UHF rectenna. This array is capable of charging IoT devices at 57 m for the LOS indoor temporal propagation model and 10 m for the LOS outdoor tropical propagation model for a transmission power of 53 dB at the base station. According to the conducted analysis, WPT can be effectively utilized in an indoor temporal region due to its extensive coverage distance. Furthermore, the paper discussed the design and measurement results of the single-element antenna employed in constructing the proposed mm-wave array. The proposed mm-wave antenna has simple geometry and high performance operating at the N257 5G band. The presented structure incorporates a multi-slot configuration consisting of three horizontally etched slots, introduced to improve the impedance bandwidth. The latter is as wide as 3.73 GHz and centered at 28 GHz. The designed antenna exhibits a stable and high in-band gain exceeding 9.5 dBi over the entire operating bandwidth, as well as wide beamwidth. These features make it suitable for body-centric applications. The configuration of antenna is planar, makes it easy for deployment and fabrication. The proposed structure has been tested in the free space and on different parts of the human model. The SAR analysis has been performed as well showing antenna compatibility with the IEEE standards.

REFERENCES

[1] M. Ur-Rehman, N. A. Malik, X. Yang, Q. H. Abbasi, Z. Zhang, and N. Zhao, "A low profile antenna for millimeter-wave body-centric applications," *IEEE Trans. Antennas Propag.*, vol. 65, no. 12, pp. 6329–6337, Dec. 2017, doi: 10.1109/TAP.2017.2700897.

[2] M. Wagih, A. S. Weddell, and S. Beeby, "Millimeter-wave power harvesting: A review," *IEEE Open J. Antennas Propag.*, vol. 1, pp. 560–578, 2020, doi: 10.1109/OJAP.2020.3028220.

[3] A. Eid, J. G. D. Hester, and M. M. Tentzeris, "Rotman lens-based wide angular coverage and high-gain semipassive architecture for ultralong range mm-wave RFIDs," *IEEE Antennas Wireless Propag. Lett.*, vol. 19, pp. 1943–1947, 2020, doi: 10.1109/LAWP.2020.3002924.

[4] M. Wagih, G. S. Hilton, A. S. Weddell, and S. Beeby, "Broadband millimeter-wave textile-based flexible rectenna for wearable energy harvesting," *IEEE Trans. Microw. Theory Techn.*, vol. 68, no. 11, pp. 4960–4972, Nov. 2020, doi: 10.1109/TMTT.2020.3018735.

[5] T. S. Rappaport, S. Sun, R. Mayzus, H. Zhao, Y. Azar, K. Wang, G. N. Wong, J. K. Schulz, M. Samimi, and F. Gutierrez, "Millimeter wave mobile communications for 5G cellular: It will work!" *IEEE Access*, vol. 1, pp. 335–349, 2013, doi: 10.1109/ACCESS.2013.2260813.

[6] A. Meredov, K. Klionovski, and A. Shamim, "Screen-printed, flexible, parasitic beam-switching millimeter-wave antenna array for wearable applications," *IEEE Open J. Antennas Propag.*, vol. 1, pp. 2–10, 2020, doi: 10.1109/OJAP.2019.2955507.

[7] D. Pozar, *Microwave Engineering*, 4th ed., Hoboken, NJ, USA: Wiley, 2011.

[8] J. Charthad, N. Dolatsha, A. Rekhi, and A. Arbabian, "System-level analysis of far-field radio frequency power delivery for mm-sized sensor nodes," *IEEE Trans. Circuits Syst. I, Reg. Papers*, vol. 63, no. 2, pp. 300–311, Feb. 2016, doi: 10.1109/TCSI.2015.2512720.

[9] T. A. Khan, A. Alkhateeb, and R. W. Heath Jr., "Millimeter wave energy harvesting," *IEEE Trans. Wireless Commun.*, vol. 15, no. 9, pp. 6048–6062, Sep. 2016, doi: 10.1109/TWC.2016.2577582.

[10] M. Tabesh, N. Dolatsha, A. Arbabian, and A. M. Niknejad, "A power-harvesting pad-less millimeter-sized radio," *IEEE J. Solid-State Circuits*, vol. 50, no. 4, pp. 962–977, Apr. 2015, doi: 10.1109/JSSC.2014.2384034.

[11] A. Eid, J. G. D. Hester, and M. M. Tentzeris, "5G as a wireless power grid," *Sci. Rep.*, vol. 11, no. 1, p. 636, Jan. 2021, doi: 10.1038/s41598-020-79500-x.

[12] M. A. S. Tajin, C. E. Amanatides, G. Dion, and K. R. Dandekar, "Passive UHF RFID-based knitted wearable compression sensor," *IEEE Internet Things J.*, vol. 8, no. 17, pp. 13763–13773, Sep. 2021, doi: 10.1109/JIOT.2021.3068198.

[13] M. Wagih, G. S. Hilton, A. S. Weddell, and S. Beeby, "Dual-band dual-mode textile antenna/rectenna for simultaneous wireless information and power transfer (SWIPT)," *IEEE Trans. Antennas Propag.*, vol. 69, no. 10, pp. 6322–6332, Oct. 2021.

[14] D. Vital, S. Bhardwaj, and J. L. Volakis, "Textile-based large area RF-power harvesting system for wearable applications," *IEEE Trans. Antennas Propag.*, vol. 68, no. 3, pp. 2323–2331, Mar. 2020, doi: 10.1109/TAP.2019.2948521.

[15] O. L. A. López, H. Alves, R. D. Souza, S. Montejo-Sánchez, E. M. G. Fernández, and M. Latva-Aho, "Massive wireless energy transfer: Enabling sustainable IoT toward 6G era," *IEEE Internet Things J.*, vol. 8, no. 11, pp. 8816–8835, Jun. 2021.

[16] U. Ullah, S. Koziel, and A. Pietrenko-Dabrowska, "Design and characterization of a planar structure wideband millimeter-wave antenna with wide beamwidth for wearable off-body communication applications," *IEEE Antennas Wireless Propag. Lett.*, vol. 21, pp. 2070–2074, 2022.

[17] A. Iqbal, A. Basir, A. Smida, N. K. Mallat, I. Elfergani, J. Rodriguez, and S. Kim, "Electromagnetic bandgap backed millimeter-wave MIMO antenna for wearable applications," *IEEE Access*, vol. 7, pp. 111135–111144, 2019, doi: 10.1109/ACCESS.2019.2933913.

[18] G. F. Hamberger, S. Trummer, U. Siart, and T. F. Eibert, "A planar dual-polarized microstrip 1-D-Beamforming antenna array for the 24-GHz band," *IEEE Trans. Antennas Propag.*, vol. 65, no. 1, pp. 142–149, Jan. 2017, doi: 10.1109/TAP.2016.2618847.

[19] U. Ullah, M. Al-Hasan, S. Koziel, and I. B. Mabrouk, "A series inclined slot-fed circularly polarized antenna for 5G 28 GHz applications," *IEEE Antennas Wireless Propag. Lett.*, vol. 20, pp. 351–355, 2021, doi: 10.1109/LAWP.2021.3049901.

[20] S. J. Chen, C. Fumeaux, Y. Monnai, and W. Withayachumnankul, "Dual circularly polarized series-fed microstrip patch array with coplanar proximity coupling," *IEEE Antennas Wireless Propag. Lett.*, vol. 16, pp. 1500–1503, 2017, doi: 10.1109/LAWP.2016.2647227.

[21] X. Lin, B.-C. Seet, F. Joseph, and E. Li, "Flexible fractal electromagnetic bandgap for millimeter-wave wearable antennas," *IEEE Antennas Wireless Propag. Lett.*, vol. 17, pp. 1281–1285, 2018, doi: 10.1109/LAWP.2018.2842109.

[22] M.-A. Chung, D. Udris, C.-W. Lin, and C.-W. Yang, "A 28-GHz Vivaldi array antenna with power divider structure for achieving wide band and gain enhancement," *Int. J. Antennas Propag.*, vol. 2024, no. 1, Jan. 2024, Art. no. 9935054, doi: 10.1155/2024/9935054.

[23] C. Renit and T. A. B. Raj, "Wearable frequency selective surface-based compact dual-band antenna for 5G and Wi-Fi applications," *Automatika*, vol. 65, no. 2, pp. 454–462, Apr. 2024, doi: 10.1080/00051144.2023.2296796.

[24] M. Wagih, G. S. Hilton, A. S. Weddell, and S. Beeby, "Millimeter-wave power transmission for compact and large-area wearable IoT devices based on a higher order mode wearable antenna," *IEEE Internet Things J.*, vol. 9, no. 7, pp. 5229–5239, Apr. 2022, doi: 10.1109/JIOT.2021.3107594.

[25] M. Zeng, A. S. Andrenko, X. Liu, Z. Li, and H.-Z. Tan, "A compact fractal loop rectenna for RF energy harvesting," *IEEE Antennas Wireless Propag. Lett.*, vol. 16, pp. 2424–2427, 2017, doi: 10.1109/LAWP.2017.2722460.

[26] C.-H.-K. Chin, Q. Xue, and C. H. Chan, "Design of a 5.8-GHz rectenna incorporating a new patch antenna," *IEEE Antennas Wireless Propag. Lett.*, vol. 4, pp. 175–178, 2005, doi: 10.1109/LAWP.2005.846434.

[27] D. K. Ghodgaonkar, O. P. Gandhi, and M. F. Iskander, "Complex permittivity of human skin in vivo in the frequency band 26.5–60 GHz," in *Proc. IEEE Antennas Propag. Soc. Int. Symp. Transmitting Waves Prog. Next Millennium. Dig. Held Conjunct. USNC/URSI Nat. Radio Sci. Meeting*, vol. 2, Salt Lake City, UT, USA, Jun. 2000, pp. 1100–1103, doi: 10.1109/APS.2000.875414.

[28] C. A. Balanis, *Antenna Theory: Analysis and Design*, 3rd ed., Hoboken, NJ, USA: Wiley, 2005, pp. 830–833.

[29] M. Wagih, O. Cetinkaya, B. Zaghari, A. S. Weddell, and S. Beeby, "Real-world performance of sub-1 GHz and 2.4 GHz textile antennas for RF-powered body area networks," *IEEE Access*, vol. 8, pp. 133746–133756, 2020, doi: 10.1109/ACCESS.2020.3011603.

[30] R. N. Tiwari, O. S. Sai, D. Sharma, M. S. Kumar, P. Singh, P. Kumar, C. Sreemanya, and S. Rajasekaran, "A low-profile dual-band millimeter wave patch antenna for high-speed wearable and biomedical applications," *Results Eng.*, vol. 24, Dec. 2024, Art. no. 103212, doi: 10.1016/j.rineng.2024.103212.

[31] C. R. Valenta, M. M. Morys, and G. D. Durgin, "Theoretical energy-conversion efficiency for energy-harvesting circuits under power-optimized waveform excitation," *IEEE Trans. Microw. Theory Techn.*, vol. 63, no. 5, pp. 1758–1767, May 2015, doi: 10.1109/TMTT.2015.2417174.

[32] T.-W. Yoo and K. Chang, "Theoretical and experimental development of 10 and 35 GHz rectennas," *IEEE Trans. Microw. Theory Techn.*, vol. 40, no. 6, pp. 1259–1266, Jun. 1992, doi: 10.1109/22.141359.

[33] S. Hemour, C. H. P. Lorenz, and K. Wu, "Small-footprint wideband 94 GHz rectifier for swarm micro-robotics," in *IEEE MTT-S Int. Microw. Symp. Dig.*, May 2015, pp. 1–4.

[34] Y. Huo, X. Dong, and W. Xu, "5G cellular user equipment: From theory to practical hardware design," *IEEE Access*, vol. 5, pp. 13992–14010, 2017, doi: 10.1109/ACCESS.2017.2727550.

[35] H. Sun, H. He, and J. Huang, "Polarization-insensitive rectenna arrays with different power combining strategies," *IEEE Antennas Wireless Propag. Lett.*, vol. 19, pp. 492–496, 2020, doi: 10.1109/LAWP.2020.2968616.

[36] G. Monti, L. Corchia, and L. Tarricone, "UHF wearable rectenna on textile materials," *IEEE Trans. Antennas Propag.*, vol. 61, no. 7, pp. 3869–3873, Jul. 2013, doi: 10.1109/TAP.2013.2254693.

[37] A. Al-Saman, M. Mohamed, M. Cheffena, and A. Moldsvor, "Wideband channel characterization for 6G networks in industrial environments," *Sensors*, vol. 21, no. 6, p. 2015, Mar. 2021, doi: 10.3390/s21062015.

[38] A. M. Al-Samman, T. A. Rahman, M. H. Azmi, and I. Shayea, "Path loss model and channel capacity for UWB–MIMO channel in outdoor environment," *Wireless Pers. Commun.*, vol. 107, no. 1, pp. 271–281, Jul. 2019, doi: 10.1007/s11277-019-06253-w.

[39] A. M. Al-Samman, T. A. Rahman, M. N. Hindia, A. Daho, and E. Hanafi, "Path loss model for outdoor parking environments at 28 GHz and 38 GHz for 5G wireless networks," *Symmetry*, vol. 10, no. 12, p. 672, Nov. 2018, doi: 10.3390/sym10120672.

[40] M. B. Majed, T. A. Rahman, O. A. Aziz, M. N. Hindia, and E. Hanafi, "Channel characterization and path loss modeling in indoor environment at 4.5, 28, and 38 GHz for 5G cellular networks," *Int. J. Antennas Propag.*, vol. 2018, pp. 1–14, Sep. 2018, doi: 10.1155/2018/9142367.

[41] G. R. Maccartney, T. S. Rappaport, S. Sun, and S. Deng, "Indoor office wideband millimeter-wave propagation measurements and channel models at 28 and 73 GHz for ultra-dense 5G wireless networks," *IEEE Access*, vol. 3, pp. 2388–2424, 2015, doi: 10.1109/ACCESS.2015.2486778.
[42] S. Sun, T. S. Rappaport, S. Rangan, T. A. Thomas, A. Ghosh, I. Z. Kovacs, I. Rodriguez, O. Koymen, A. Partyka, and J. Jarvelainen, "Propagation path loss models for 5G urban micro- and macro-cellular scenarios," in *Proc. IEEE 83rd Veh. Technol. Conf. (VTC Spring)*, May 2016, pp. 1–6.

FUAD ERMAN was born in Palestine. He received the B.Eng. degree in electronics and communications engineering from Al-Baath University, in 2013, the M.Sc. degree in communication and network engineering from the University of Putra Malaysia, in 2017, and the Ph.D. degree in electrical engineering from the University of Malaya, in 2020. He was with the Engineering Optimization and Modeling Center (EOMC), School of Science and Engineering, Reykjavik University, Iceland, from 2022 to 2023. He is currently an Assistant Professor with the College of Telecommunications and Information Technology, Nablus University for Vocational and Technical Education, Nablus, Palestine. His current research interests include RFID antennas and wearable antennas.

SLAWOMIR KOZIEL (Fellow, IEEE) received the M.Sc. and Ph.D. degrees in electronic engineering from Gdansk University of Technology, Poland, in 1995 and 2000, respectively, the dual M.Sc. degree in theoretical physics and mathematics, in 2000 and 2002, respectively, and the Ph.D. degree in mathematics from the University of Gdansk, Poland, in 2003. He is currently a Professor with the Department of Engineering, Reykjavik University, Iceland. His research interests include CAD and modeling of microwave and antenna structures, simulation-driven design, surrogate-based optimization, space mapping, circuit theory, analog signal processing, evolutionary computation, and numerical analysis.

ALHARETH ZYOUD (Member, IEEE) received the bachelor's degree in electrical engineering from Palestine Polytechnic University, in 2006, and the master's and Ph.D. degrees in communication engineering from International Islamic University, Malaysia, in 2011 and 2017, respectively. He is currently an Assistant Professor with the Department of Electrical and Computer Engineering, Birzeit University, Palestine. He has authored or co-authored many research papers in international journals and conferences. His current research interests include RF modeling and simulation, 5G radio resource management, and energy management.

LEIFUR LEIFSSON received the bachelor's and master's degrees in mechanical engineering from the University of Iceland, Reykjavik, Iceland, in 1999 and 2000, respectively, and the Ph.D. degree in aerospace engineering from Virginia Tech, Blacksburg, VA, USA, in 2006. He is currently an Associate Professor of aerospace engineering with Purdue University, West Lafayette, IN, USA. His research interests include computational modeling, optimization, and uncertainty quantification of engineered systems with an emphasis on methods for multifidelity modeling and machine learning. His current application areas include aerodynamic shape optimization, aerodynamic flutter, model-based nondestructive evaluation, microwave devices, and food-energy-water nexus.

UBAID ULLAH (Senior Member, IEEE) received the M.Sc. and Ph.D. degrees in electrical and electronic engineering from Universiti Sains Malaysia, in 2013 and 2017, respectively. During his Ph.D., he was awarded the prestigious Global Fellowship and the Outstanding Student Award. He was with the Engineering Optimization and Modeling Center, School of Science and Engineering, Reykjavik University, Iceland, from 2017 to 2019. He is currently an Assistant Professor with the Network and Communication Engineering Department, Al Ain University, Abu Dhabi, United Arab Emirates. His research interests include antenna theory, small antennas, antenna polarization, dielectric resonators, waveguides, millimeter-wave antenna designs, multiple-input multiple-output (MIMO) antenna systems, metamaterials, EM-simulation-driven design, numerical analysis, microwave circuit design, and optimization.

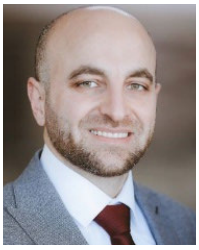

SHAKER ALKARAKI (Member, IEEE) received the B.Sc. degree (Hons.) in communication engineering from International Islamic University Malaysia (IIUM), Kuala Lumpur, Malaysia, in 2011, the M.Sc. degree (Hons.) from The University of Manchester (UoM), Manchester, U.K., in 2013, and the Ph.D. degree in electronic engineering from the Queen Mary University of London (QMUL), London, U.K., in 2019. From June 2019 to March 2023, he was a Postdoctoral Researcher with the Antennas and Electromagnetics Group, QMUL. He is currently an Assistant Professor with the George Green Institute for Electromagnetics Research, Department of Electrical and Electronic Engineering, University of Nottingham, Nottingham, U.K. Up to date he authored more than 55 Journal and conference papers and three book chapters. His research interests and experience are interdisciplinary in nature and are at the intersection between antennas, microwave, millimeter-wave (mm-wave) engineering, wireless communications, 3D printing, and material sciences, such as using liquid metal for the development of novel devices. This also includes: mm-wave and microwave-reconfigurable devices, mm-wave antennas and arrays, 3-D-printed antennas, 5G antennas and systems, multiple-input and multiple-output (MIMO) systems, leaky waves, liquid metal antennas, and microwave devices. He received the B.Sc. Scholarship from IIUM, the M.Sc. Scholarship from Hani Qaddumi Scholarship Foundation, and the Ph.D. Scholarship from QMUL.